by stepping the telescope at the end of each right ascension scan. A 2.1–arc sec square aperture was used for mapping, but the step size was 1 arc sec in both directions to provide Nyquist sampling. Several successive scans of the planet were made and subsequently added together to improve the signal-to-noise ratio. The sky brightness and the different zero points of the 16 detectors were estimated from measurements of the sky in the corners of each image and subtracted from the images. To reduce the effects of scattered sunlight from the bright crescent, we subtracted an appropriately scaled out-of-band image, taken at a wavelength where the Venus night side produces little radiation.

14. The first model was identical to that described by Bell *et al.* (*5*). The δEddington/Adding algorithm was used to solve the equation of transfer in an absorbing, emitting, scattering atmosphere [D. Crisp, *Icarus* **67**, 484 (1986)]. Monochromatic gas absorption coefficients were computed on a 0.01 cm^{-1} grid with a modified version of the line-by-line model described by D. Crisp [*J. Geophys. Res.* **95**, 14577 (1990)]. The model atmosphere was divided into 50 vertical layers between the surface and 100 km.
15. The second model was developed by B. Dalton at NASA Ames Research Center. It is based on a two-stream source function solution to the equation of transfer [O. B. Toon, J. B. Pollack, C. Sagan, *Icarus* **30**, 663 (1977); O. B. Toon, C. P. McKay, T. P. Ackerman, K. Santhanam, *J. Geophys. Res.* **94**, 16287 (1989)] and uses monochromatic gas absorption coefficients from FASTCODE [S. A. Clough, F. X. Kneizys, L. S. Rothman, W. O. Gallery, *SPIE* **277**, *Atmospheric Transmission*, 152 (1981)]. The spectral resolution was 0.1 cm^{-1}. The model atmosphere was divided into 22 vertical layers.
16. L. Rothman *et al.*, *Appl. Opt.* **26**, 4085 (1987); N. Husson *et al.*, *Ann. Geophys.* **4**, 185 (1986).
17. For CO_2, we adopted an approach similar to that described by Bezard *et al.* (*4*) and augmented the line parameters on the 1986 version of the HITRAN database with weaker transitions listed by L. S. Rothman [*Appl. Opt.* **25**, 1795 (1986)]. The band parameters for H_2O and CO were taken directly from the HITRAN database. The spectral line parameters for the OCS $2\nu_3$ band at 2.45 μm were taken from L. R. Brown *et al.*, *ibid.* **26**, 5154 (1987)]. In addition, we included collision-induced absorption by CO_2 by combining the absorption coefficients given by J. F. Moore [*Rep. X-630-72-48* (NASA Goddard Space Flight Center, Greenbelt, MD, 1971)] with a wavelength-independent component of 4×10^{-8} cm^{-1} amagat^{-2}. The latter source of continuum opacity was needed to produce an adequate fit to the shape of the spectrum at wavelengths between 2.15 and 2.3 μm, where CO_2 and the H_2CO_4 cloud particles are the only known sources of extinction. It has no known theoretical justification, but it may compensate for errors introduced by uncertainties in the shapes of the far wings of CO_2 lines or other factors.
18. The new database was constructed from solutions to the quantum mechanical equations based on the direct numerical diagonalization (DND) technique [R. B. Wattson and L. S. Rothman, *J. Mol. Spectrosc.* **119**, 83 (1986)]. The DND method yields line positions that are accurate to a 0.01 cm^{-1} and line intensities with accuracies exceeding 10%.
19. A. Seiff, in *Venus*, D. M. Hunten, L. Colin, T. M. Donahue, V. I. Moroz, Eds. (Univ. of Arizona Press, Tucson, 1983), pp. 215–279.
20. D. Crisp, *Icarus* **67**, 484 (1986). The main cloud deck consists of upper (57 to 70 km), middle (49 to 57 km), and lower (47 to 49 km) layers, each containing mixtures of H_2SO_4 droplets with the four distinct particle size populations described by R. G. Knollenberg and D. M. Hunten [*J. Geophys. Res.* **85**, 8039 (1980)]: mode 1 (0.3 μm), mode 2 (1.0 μm), mode 2′ (1.4 μm), and mode 3 (3.6 μm). The numbers in parentheses give the modal particle radius. A Mie-scattering model (J. B. Pollack *et al.*, *ibid.*, p. 8141) was used to derive the wavelength-dependent optical properties of each particle mode from the optical constants of liquid H_2SO_4 [K. F. Palmer and D. Williams, *Appl. Opt.* **14**, 208 (1975)]. Log-normal size distributions were used for all modes.
21. P. J. Connes *et al.*, *Astrophys. J.* **233**, L29 (1979).
22. J.-P. Parisot and G. Moreels, *Icarus* **42**, 46 (1980).
23. Y. L. Yung and W. B. Demore, *ibid.* **51**, 199 (1982).
24. This work was funded in part by grants from the NASA Planetary Astronomy and Planetary Atmospheres Programs to the Jet Propulsion Laboratory, California Institute of Technology, and the NASA Ames Research Center. Much of the computer time was provided by the Wide-Field–Planetary Camera II Project at the Jet Propulsion Laboratory. We thank B. Dalton for developing and assisting in the use of the computer program for the second model (*15*) and for running some of the simulations presented here. We thank the AAT Time Allocation Committee for awarding the observing time for this program.

19 March 1991; accepted 21 June 1991

Climatic Change in Tasmania Inferred from a 1089-Year Tree-Ring Chronology of Huon Pine

EDWARD COOK, TREVOR BIRD, MIKE PETERSON, MIKE BARBETTI, BRENDAN BUCKLEY, ROSANNE D'ARRIGO, ROGER FRANCEY, PIETER TANS

A climatically sensitive huon pine tree-ring chronology from western Tasmania allows inferences about Austral summer temperature change since A.D. 900. Since 1965, huon pine growth has been unusually rapid for trees that are in many cases over 700 years old. This growth increase correlates well with recent anomalous warming in Tasmania on the basis of instrumental records and supports claims that a climatic change, perhaps influenced by greenhouse gases, is in progress. Although this temperature increase exceeds any that are inferred to have occurred during the past 1089 years at this location, it has not yet clearly emerged from the natural background variability of climate in this part of the Southern Hemisphere.

COMPARED TO THE INSTRUMENTAL and historical climate records of the Northern Hemisphere (*1*), the Southern Hemisphere has relatively few high-resolution climatic time series that extend back more than 100 years (*2*). Yet, to evaluate properly recent climatic trends and fluctuations, especially for changes that might be induced by radiatively active trace gases, much longer records are needed (*3*). To help fulfill this need, we developed a climatically sensitive tree-ring chronology from Tasmania that extends back to A.D. 900.

The tree-ring site is a disjunct, subalpine stand of huon pine (*Lagarostrobus franklinii* C. J. Quinn) located at 950-m elevation on Mount Read, a 1124-m-high massif located in western Tasmania (Fig. 1) that projects above the local timberline. In all, 56 radii from 23 trees were sampled and processed for tree-ring analysis with the use of established methods (*4, 5*). After cross-dating and measurement, the ring-width series were standardized (*6*) to remove long-term growth trends attributed to increasing tree size and maturation. This approach was taken in order to avoid removing any long-term climatic variance that was potentially distinguishable from purely biological growth trends. We then averaged the standardized tree-ring indices using a robust mean to discount the influence of outliers (*6*). The result was a mean site chronology that covered the interval A.D. 900 to 1988 (Fig. 2).

Both very poor and very rapid growth periods have occurred over the past 100 years in the huon pine chronology. Growth was poor from 1898 to about 1913; four of the nine poorest years of accumulated growing degree-days since 1870 in Canterbury, New Zealand (*7*), occurred during this period, and it overlaps with part of the coldest period (1900 to 1935) in recorded New Zealand history (*8*). It also coincides with the occurrence of a cold sea-surface temperature (SST) anomaly off the west coast of Tasmania (*9, 10*) that presumably contributed to reduced air temperatures over the island and reduced tree growth at other subalpine sites on the island (*11*). Growth has been unusually rapid since 1965 and parallels recent temperature increases in New Zealand (*8*), warm SSTs around Tasmania (*10*), and increased warming throughout much of the Southern Hemisphere (*12, 13*).

These apparent temperature changes were statistically modeled by comparing the huon

---

E. Cook, B. Buckley, R. D'Arrigo, Tree-Ring Laboratory, Lamont-Doherty Geological Observatory, Palisades, NY 10964.
T. Bird, Tasmanian Trades and Labour Council, Forestry Unit, New Town, Tasmania 7008, Australia.
M. Peterson, Tasmania Forestry Commission, Hobart, Tasmania 7001, Australia.
M. Barbetti, N. W. G. Macintosh Centre, University of Sydney, New South Wales 2006, Australia.
R. Francey, Commonwealth Scientific and Industrial Research Organization (CSIRO), Division of Atmospheric Research, Mordialloc, Victoria 3195, Australia.
P. Tans, Climate Monitoring and Diagnostics Laboratory, National Oceanic and Atmospheric Administration, Boulder, Colorado 80309.

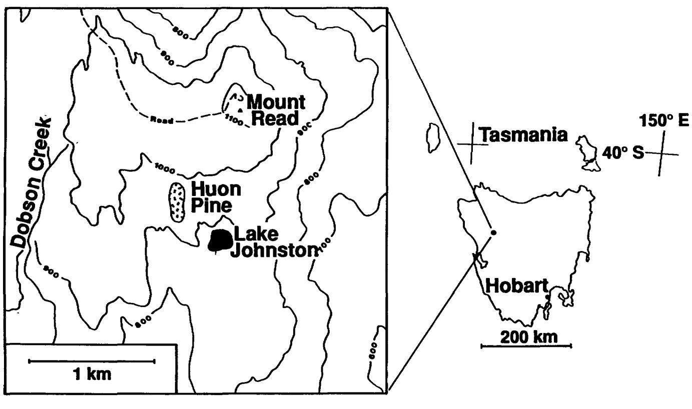

Fig. 1. Map of Tasmania and locations of Lake Johnston and the huon pine tree-ring site on Mount Read.

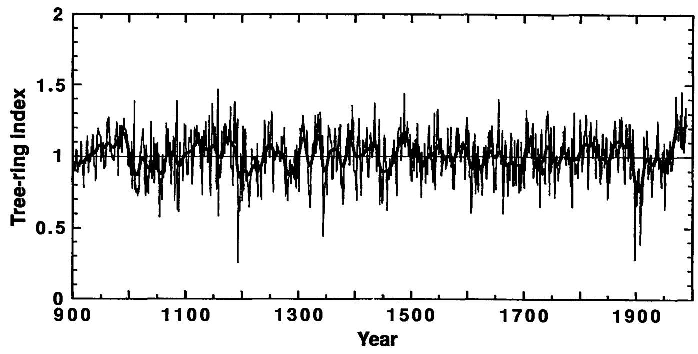

Fig. 2. The Lake Johnston huon pine tree-ring chronology. The time span is A.D. 900 to 1988, inclusive. The smoothed curve superimposed on the annual tree-ring indices emphasizes fluctuations of 20 or more years in duration.

pine chronology with long mean monthly temperature records from three Tasmanian meteorological stations: Hobart (1883 to 1989), Launceston (1885 to 1989), and Low Head Lighthouse (1895 to 1989). Only the 1895 to 1989 period common to all stations was used for analysis. Before 1895, the temperature data appear to be seriously inhomogeneous. We computed correlations between huon pine tree rings and Tasmania temperatures for the months of October to May, which include the current growing season, using the original tree-ring indices (Fig. 2), a prewhitened chronology of residuals obtained by modeling and removing autoregressive persistence (*14*) from the indices, and a chronology of first-differenced indices. The last two chronologies emphasize in different ways the high-frequency growth variations; they thus make the determination of statistical significance more robust. For comparison with the tree-ring residuals and first-differences, the monthly temperatures were similarly prewhitened and differenced. The common time period used to compute the correlations was 1896 to 1988, which provided 91 degrees of freedom for testing.

Positive correlations are seen for November through April that meet or exceed the 95% and, in most instances, the 99% confidence limits (Fig. 3). There is also relatively little difference among the patterns of the original, residual, and first-differenced correlations. This similarity indicates that autocorrelation has not seriously inflated the indicated temperature signal in the original chronology. This stability implies that current growing season temperatures and huon pine growth are causally linked.

Comparison of the best correlated November–April temperatures averaged into one season and the huon pine chronology indicate the degree to which the recent growth fluctuations have probably been caused by climate (Fig. 4). Each series was smoothed in order to emphasize decadal-scale fluctuations and longer term trends. The correlations between the unsmoothed temperatures and the original, prewhitened, and first-differenced tree-ring indices were 0.60, 0.51, and 0.49, respectively, a result highly consistent with the earlier monthly correlation analyses. In contrast, the correlation between the smoothed curves is 0.82, which is high enough to indicate that the low-frequency temperature signal in the tree rings is real. This result was validated with the use of cross-spectral analysis (*15*), which indicated that there is statistically significant ($\alpha < 0.05$) coherence at all periods greater than 12 years. Thus, changing warm season temperatures appear to be largely responsible for the observed huon pine growth fluctuations, especially the growth increase since 1965.

With its statistically modeled temperature signal, our huon pine chronology is one of the longest high-resolution paleoclimatic records from the Southern Hemisphere. Among its many uses, it allows the recent climatic warming in Tasmania to be placed in context with 1089 years of temperature change. From Fig. 2, it is apparent that the temperature increase since 1965 is anomalous compared to most earlier periods of comparable duration. Of the earlier periods that include some years of comparable warmth, the most notable were A.D. 940 to 1000, 1100 to 1190, and 1475 to 1495. Interestingly, the period from A.D. 1100 to 1190 was contemporaneous with the Medieval Warm Epoch (*16*), which has been considered to have been the warmest event since A.D. 1000 in the Northern Hemisphere. However, neither in that epoch nor in any other period has Tasmania been as consistently warm as it has been since 1965 on the basis of our tree-ring record. This finding lends credence to some claims that recent hemispheric and global temperature increases are being driven by the greenhouse effect. We do not consider our results as added proof of that assertion yet, because the recent warming still appears to be within the range of natural low-frequency variabil-

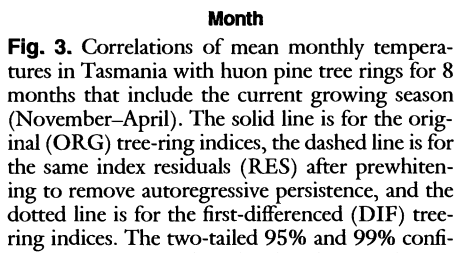

Fig. 3. Correlations of mean monthly temperatures in Tasmania with huon pine tree rings for 8 months that include the current growing season (November–April). The solid line is for the original (ORG) tree-ring indices, the dashed line is for the same index residuals (RES) after prewhitening to remove autoregressive persistence, and the dotted line is for the first-differenced (DIF) tree-ring indices. The two-tailed 95% and 99% confidence limits are only valid for the correlations based on the prewhitened and differenced data. Note the significant positive response to current growing season temperatures.

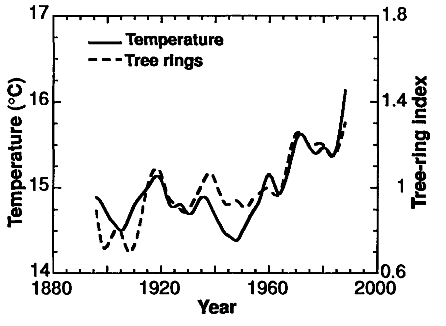

Fig. 4. Comparisons of November–April average temperatures for Tasmania with the original huon pine tree-ring indices. The data have been smoothed to emphasize decadal fluctuations and longer trends.

ity seen in the complete record.

The huon pine chronology also reveals numerous past episodes of persistently above- and below-average summer temperatures lasting ten or more years. Yet the coldest and warmest periods inferred from our tree-ring record apparently occurred within about 50 years of each other in the 20th century. This pattern of unusual cold followed by unusual warmth could strongly skew the evaluation of recent temperature trends in Southern Hemisphere instrumental records, which are relatively infrequent before 1900 (*13*). As this study shows, long, high-resolution paleotemperature records from the Southern Hemisphere can help in properly evaluating the current warming trend.

In many respects the cold event of the early 1900s is as interesting as the post-1965 warming in Tasmania. It is present in both land and marine instrumental temperature records covering much of the Southern Hemisphere (*7–10, 13, 17–19*). The temperature decline was apparently preceded by a circumpolar expansion of Antarctic pack ice and the irruption of numerous icebergs into normally ice-free low latitudes (*20*). Other manifestations of this anomaly were a decrease in scalar wind speed in the Tasmania–New Zealand sector (*17*) and circumpolar changes in middle latitude (40° to 50°S) sea-level pressure associated with oscillations in zonal flow with a wave number of zero (*21*). Thus, there appears to have been a significant reorganization of the Southern Hemisphere ocean-atmosphere system in the early 1900s. A similar event of lesser magnitude may have also occurred around A.D. 1190 on the basis of qualitatively similar changes in the huon pine record. Understanding the mechanisms responsible for these and other past climatic fluctuations could contribute greatly toward explaining the recent warming in the Southern Hemisphere.

REFERENCES AND NOTES

1. H. H. Lamb, *Climate: Past, Present, and Future* (Methuen, London, 1977), vol. 2.
2. R. G. Barry, in *Climatic Change and Variability*, A. B. Pittock, L. A. Frakes, D. Jenssen, J. A. Peterson, J. W. Zillman, Eds. (Cambridge Univ. Press, London, 1978), pp. 150–166.
3. R. A. Bryson, *Science* **184** , 753 (1974).
4. H. C. Fritts, *Tree Rings and Climate* (Academic Press, London, 1976).
5. J. R. Pilcher *et al.*, in *Methods of Dendrochronology*, E. R. Cook and L. A. Kairiukstis, Eds. (Kluwer, Dordrecht, 1989), pp. 40–50.
6. E. R. Cook *et al.*, in *ibid.*, pp. 104–123.
7. M. J. Salinger, *Clim. Change* **2**, 109 (1979).
8. ——— and J. M. Gunn, *Nature* **256**, 396 (1975).
9. C. K. Folland, D. E. Parker, F. E. Kates, *ibid.* **310**, 670 (1984).
10. M. Bottomley *et al.*, *Global Ocean Surface Temperature Atlas* (Meteorological Office, Bracknell, U.K., 1990).
11. J. Ogden, *Tree-Ring Bull.* **38**, 1 (1978).
12. G. Paltridge and S. Woodruff, *Mon. Weather Rev.* **109**, 2427 (1981).
13. P. D. Jones, S. C. B. Raper, T. M. L. Wigley, *J. Clim. Appl. Meteorol.* **25**, 1213 (1986).
14. G. E. P. Box and G. M. Jenkins, *Time Series Analysis: Forecasting and Control* (Holden-Day, San Francisco, 1976).
15. G. M. Jenkins and D. G. Watts, *Spectral Analysis and Its Applications* (Holden-Day, San Francisco, 1968).
16. H. H. Lamb, *Palaeogeogr., Paleoclimatol. Paleoecol.* **1**, 13 (1965).
17. J. O. Fletcher, U. Radok, R. Slutz, *J. Geophys. Res.* **87**, 4269 (1982).
18. A. H. Oort, Y. H. Pan, R. W. Reynolds, C. F. Ropelewski, *Clim. Dynam.* **2**, 29 (1987).
19. J. Hansen and S. Lebedeff, *J. Geophys. Res.* **92**, 13,345 (1987).
20. C. J. Burrows, *N. Z. Geogr.* **32**, 127 (1976).
21. H. Enomoto, *Clim. Change* **18**, 67 (1991).
22. We thank the Climate Center of Lamont-Doherty Geological Observatory, the National Science Foundation Division of Climate Dynamics (grant ATM 89-15353), the NOAA Climate and Global Change Program (grant NA 98AA-D-AC199), the CSIRO Division of Forestry and Forest Products, and the Tasmania Forestry Commission for research support; and W. S. Broecker, M. Cane, G. Jacoby, D. Peteet, and two anonymous reviewers for critical reviews. Lamont-Doherty Geological Observatory Contribution No. 4824.

18 April 1991; accepted 24 June 1991

Rel-Associated pp40: An Inhibitor of the Rel Family of Transcription Factors

Nathan Davis,* Sankar Ghosh,*† Daniel L. Simmons,
Paul Tempst, Hsiou-chi Liou, David Baltimore, Henry R. Bose, Jr.

The Rel-associated protein pp40 is functionally related to IκB, an inhibitor of the transcription factor NF-κB. Purified pp40 inhibits the DNA binding activity of the NF-κB protein complex (p50:p65 heterodimers), p50:c-Rel heteromers, and c-Rel homodimers. The sequence of the complementary DNA encoding pp40 revealed similarity to the gene encoding MAD-3, a protein with mammalian IκB-like activity. Protein sequencing of IκB purified from rabbit lung confirmed that *MAD-3* encodes a protein similar to IκB. The sequence similarity between MAD-3 and pp40 includes a casein kinase II and consensus tyrosine phosphorylation site, as well as five repeats of a sequence found in the human erythrocyte protein ankyrin. These results suggest that *rel*-related transcription factors, which are capable of cytosolic to nuclear translocation, may be held in the cytosol by interaction with related cytoplasmic anchor molecules.

The products of the proto-oncogene c-*rel* and the *rel* viral oncogene are members of a family of transcription factors that include the two subunits of transcription factor NF-κB (p50 and p65) and the *Dro-sophila* maternal morphogen *dorsal* (*1–4*). These proteins share sequence homology over 300 amino acids at their NH_2-terminus, a region that includes the DNA binding and dimerization domains. These proteins specifically bind to DNA sequences that are the same or slight variations of the 10-bp κB sequence in the immunoglobulin κ light chain enhancer. This κB binding sequence is present in a number of cellular and viral enhancers, and c-*rel* associates with these sites in the human immunodeficiency provirus (*5*).

Among the Rel-related proteins, NF-κB has been studied most extensively. NF-κB, a heterodimer of p50 and p65 subunits (*6*), is present ubiquitously in an inactive form in the cytosol, but is a constitutively active, nuclear protein in mature B cells (*7*). The DNA binding activity of NF-κB is activated and rapidly transported to the nucleus in cells exposed to mitogens or growth factors (*6–9*). The inactive cytosolic form is bound to IκB, which was initially characterized as a protein that specifically inhibits DNA binding by NF-κB (*8*). Purification of IκB from cell extracts reveals two forms, the major form of 35 to 37 kD (IκB-α) and a minor form of 40 to 45 kD (IκB-β) (*10, 11*). Treatment with the detergent deoxycholate (DOC) disrupts this NF-κB:IκB complex, releasing NF-κB, which then binds to DNA (*8*). Thus NF-κB may act as a second messenger, as the stimulatory signals initiated at the cell surface are transduced to the nucleus through the phosphorylation of IκB.

The products of c-*rel* and v-*rel* are found in the cytosol of avian lymphocytes associated with a distinct set of cellular proteins (pp40, p70, p115, and p124) (*12–16*). The molecular size of the 40-kD phosphoprotein (pp40) is close to that of IκB. In addition,

N. Davis and H. R. Bose, Jr., Department of Microbiology and Cell Research Institute, University of Texas at Austin, Austin, TX 78712.
S. Ghosh and H.-C. Liou, Whitehead Institute for Biomedical Research, Cambridge, MA 02142.
D. L. Simmons, Department of Chemistry, Brigham Young University, Provo, UT 84602.
P. Tempst, Memorial Sloan Kettering Cancer Center, New York, NY 10021.
D. Baltimore, Whitehead Institute for Biomedical Research, Cambridge, MA 02142, and Rockefeller University, New York, NY 10021.

---

*The first two authors contributed equally to this work.

†Present address: Section of Immunobiology, Yale University School of Medicine, New Haven, CT 06510.